FINITE ELEMENT ANALYSIS OF INDIVIDUAL WOOD-PULP FIBERS SUBJECTED TO TRANSVERSE COMPRESSION

Behrouz Shiari

Research Associate
Department of Mechanical and Aerospace Engineering
Carleton University
Ottawa, Ontario, Canada K1S 5B6

and

*Peter M. Wild**

Associate Professor
Department of Mechanical Engineering
University of Victoria
Victoria, BC, Canada V8W 3P6

(Received June 2002)

ABSTRACT

The nonlinear and large displacement finite element method has been used to perform computer simulations of the transverse collapse of single wood-pulp fibers. Initial uncollapsed cross-sectional geometries are defined based on the collapsed geometry of single fibers subjected to experimental transverse compression. These initial uncollapsed geometries are assumed to be either square-formed or circle-formed. The fiber material is assumed to be isotropic and elastic. The elastic modulus is taken as the equivalent transverse elastic modulus for the fiber wall, determined from the slope of the cell-wall compression part of the experimental collapse curve. Simulations of the deformation of fibers under transverse compression yield upper and lower bounds on experimental data. Parametric studies of the effects of fiber wall thickness, uncollapsed thickness, and elastic modulus on collapse behavior are also presented.

Keywords: Fibers, compression, finite element, collapse.

INTRODUCTION

The collapse behavior of wood-pulp fibers, its dependence on mechanical and chemical treatments, and its effect on the papermaking process have been the subject of a number of studies. Most of these studies have used experimental methods to characterize collapse behavior.

Hartler and Nyrén (1969) studied single fiber compression using an instrument in which fibers were pressed between two parallel, optically flat glass plates. The typical load-deformation curve of a single fiber under an increasing force was found to be as shown in Fig. 1. Nyrén identified two regions in this typical collapse curve: (1) collapse of the lumen; and (2) compression of the fiber wall. A "knee" in the curve characterizes the transition from lumen collapse to fiber-wall compression.

Reizin'sh and Chernyavskaya (1975) also studied the effects of transverse loading using an instrument similar to Nyrén's. The typical force versus displacement curve that they describe is similar to Nyrén's.

Amiri and Hofman (2003) used impact testing on pulp pads to simulate the compression of pulp in refining. It was found that pulp mat compression could be divided into the three regions corresponding to the three regions of fiber collapse described by Nyrén.

Hardacker (1969) studied the effects of transverse compression on fiber width. Fibers were placed between two optically flat, clear, synthetic sapphire anvils. Width was measured with the aid of an image-splitting optical microscope.

* Corresponding author (pwild@uvic.ca).

Wood and Fiber Science, 36(2), 2004, pp. 135–142
© 2004 by the Society of Wood Science and Technology

It was found that the fiber width remained relatively constant except at high loading where plastic flow begins.

Luce (1970) performed a series of tests on large models having round, tubular shapes to simulate fibers of various kinds. He found that fiber dimensions are paramount to transverse fiber properties, specifically fiber width and wall thickness. The force to collapse the fiber was shown to be related to squares of inside and outside diameters of the fiber model.

In addition to the experimental studies discussed above, one study has been identified in which the behavior or fibers under transverse loading is analyzed with the aid of numerical methods. Thorpe and McLean (1983) used the commercial finite element analysis (FEA) software, COSMOS, to develop three-dimensional linear finite element models of fibers subjected to compressive and shear stresses. The fiber cross-sections were represented with rectangular external profiles and circular lumen profiles. The fiber wall was modeled in three layers corresponding to the primary-middle lamella region and the S1 and S2 layers. Each layer was modeled with a single element depth of 8-noded brick elements having orthotropic properties based on data from the literature. Compressive and shear stresses were exerted upon the model, resulting in strains of up to 83%. It was suggested that these strains would cause splitting and cracking in the S2 layer, resulting in a collapse of the fiber structure. The validity of these models is questionable, however, as linear FEA does not accurately capture behaviors in which there are large deflections and strains, as is the case in fiber collapse.

In addition to the experimental and numerical studies discussed above, Jang and Seth (1998, 2001) have used confocal laser scanning microscopy to characterize cross-sectional images of fibers, particularly the state of lumen collapse. They derived a Collapse Index, calculated from the measured lumen area and calculated uncollapsed area, assuming the uncollapsed cross-section is either circular or rectangular. A semi-empirical model was developed that related this Collapse Index to fiber geometry, properties and, applied transverse load. However, the relationship between transverse force, Collapse Index, and the geometry factors has yet to be verified.

Nonlinear finite element modeling is widely used in the analysis of nonlinear mechanical systems. Applications include metal forming, biomechanics, soil mechanics, and elastomers. There are, in general, three classes of nonlinearities that these methods address: material (e.g., plasticity, nonlinear elasticity, visco-elasticity), geometric (e.g., large defection, large strain, buckling), and change of status (e.g., contact). None of the studies discussed above makes use of nonlinear finite element modeling to the analysis of the collapse of single wood-pulp fibers. In this work, the commercial finite element software ANSYS is used to model the collapse of a single fiber subjected to transverse compression. Cross-sectional geometry and material properties for the model are taken from experimental collapse data for individual fibers. The modeled force versus displacement data is then compared to the experimental force versus displacement data for that fiber.

GEOMETRY AND MECHANICAL PROPERTIES FOR THE MODEL

The geometry, internal structure, and material properties of wood-pulp fibers are complex, and the model presented here captures only the most macroscopic of those features. For each model, the geometry and material properties are based on experimental fiber collapse data for a corresponding never-dried kraft black spruce fiber. These data were collected using the fiber collapse instrument developed by Dunford and Wild (2002). All tests were conducted at ambient temperature, and the fibers were maintained in the wet state. Three fibers were selected whose force versus displacement curves clearly showed the regions of lumen collapse, transition, and cell-wall compression, as shown in Fig. 1.

Development of the fiber model requires unique identification of the point of collapse. Hartler and Nyrén (1969) identified the collapse point as the intersection of tangents to the cell-wall compression and lumen collapse regions of the curve, as shown in Fig. 1. The tangent to the

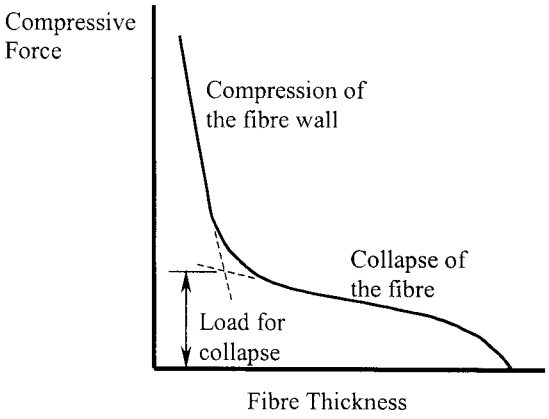

FIG. 1. Typical force versus displacement curve for fiber compression (after Hartler and Nyrén [1969]).

cell-wall compression region is relatively insensitive to where the tangent is taken. However, the tangent to the lumen collapse region is very sensitive to where the tangent is taken. In addition, for fibers that are partially collapsed, this collapse region of the curve is incomplete. For these reasons, the collapse point determined by this method is somewhat arbitrary. Furthermore, the collapse point itself is not on the curve. In order to identify a collapse force and a collapse thickness that coincide, the intersection of tangents must somehow be extrapolated to a point on the curve. Because of these shortcomings, an alternative method for determination of the collapse point was developed.

In this alternative method, the point of collapse was assumed to be the point at which the angle between the tangent to the force displacement curve and the horizontal axis was 50% of the angle in the region of cell-wall compression, as shown in Fig. 2. This method depends only on the tangent to the cell-wall compression region which, as noted above, is less sensitive to where the tangent is taken. It is recognized that this point may not coincide with the actual collapse point, but it is a relatively consistent means by which to determine an estimated value.

To estimate the geometry of the uncollapsed fiber, it is assumed that the shape of the fiber at the point of collapse is as shown in Fig. 3(a), where t_c is the thickness of the fiber and w is the width of the fiber. It is further assumed that the perimeter of the fiber cell wall and the cell-wall thickness ($t_w = t_c/2$) are both preserved during fiber collapse. The dimensions of the uncollapsed fiber are then as shown in Figs. 3(b) and 3(c) for initially square and circular fiber cross-sections, respectively.

The width of the fiber, w, is determined using an optical microscope after the fiber has been subjected to the compressive test. The width measured in this manner is likely somewhat different from the width of the fiber at the collapse

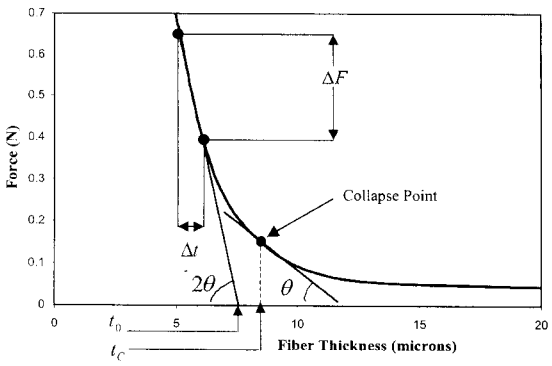

FIG. 2. Determination of collapse point and of equivalent elastic modulus of the cell wall.

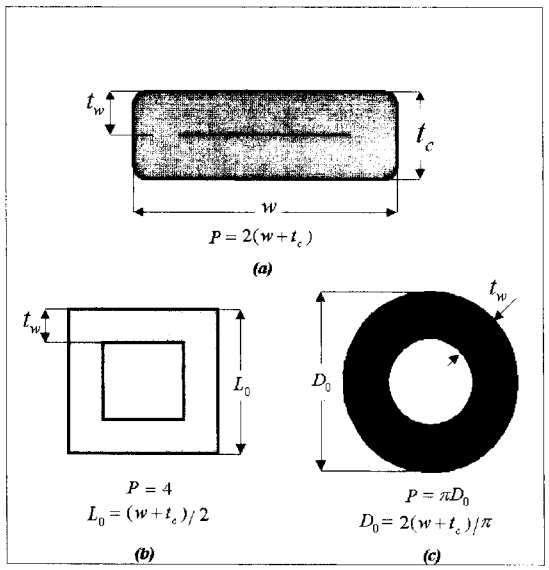

FIG. 3. Circle-formed and square-formed fiber geometries.

point during the compression test. However, as found by Hardracker (1969), the width of a fiber does not vary appreciably under transverse compression.

The cell-wall material is assumed to be uniform (i.e., nonlayered) and isotropic. This material is further assumed to be linear elastic and the modulus is assumed to be equal to the equivalent elastic modulus, E_e, of the cell-wall compression portion of the experimental collapse curve for the fiber, as defined by Dunford and Wild (2002).

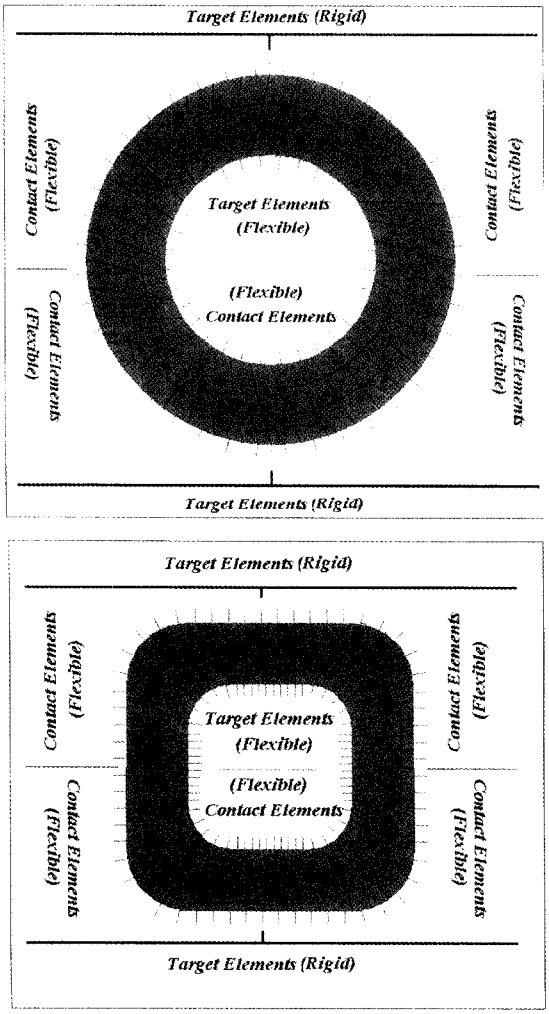

FIG. 4. FEA models.

$$E_e = \frac{\Delta F t_0}{\Delta t \; A} \tag{1}$$

Here, t_0 is the reference fiber thickness, as shown in Fig. 4, A is the area of the fiber that is being compressed, and $\Delta F/\Delta t$ is the slope of the force versus displacement curve, as shown in Fig. 2. The area of fiber compression, A, is the product of the fiber width, w, and the diameter of the probes between which the fibers are compressed in the compression instrument.

THE FINITE ELEMENT MODEL

As discussed in the introduction, nonlinear FEA can be used to capture material, geometric, and change of status nonlinearities. The fiber model developed here includes large displacement nonlinearities associated with the significant motions of the cell wall during lumen collapse. The model also includes change of status nonlinearities in the form of contact between the compression surfaces and the fiber and between opposing surfaces of the lumen. The model does not include nonlinearities associated with the behavior of the fiber material itself. The model is based on an isotropic elastic material, as discussed in the previous section.

Model geometry for the uncollapsed fibers was determined as discussed in the section above and illustrated in Fig. 3. This geometry was meshed with four-noded, 2-dimensional, axisymmetric solid elements (ANSYS element Plane42). The mesh was defined parametrically to facilitate modification of the mesh density. Sensitivity studies of alternative mesh densities were conducted to ensure that the mesh was sufficiently dense. Meshes for the circle-formed and square-formed models of a fiber are shown in Fig. 4.

The surfaces of the compression instrument that contact the fiber are modeled as rigid bodies. Contact between the outside surface of the fiber and the compression instrument is modeled with contact *element pairs,* as shown in Fig. 4. Contact pairs consist of a contact element (ANSYS CONTA172 Element) on one body and a target element (ANSYS TARGE169 Element) on the other. Similarly, pairs of contact elements

TABLE 1. *Geometric parameters for test data and equivalent FEA models.*

	Width (μm)	Thickness at collapse (μm)	Equivalent Young's modulus (MPa)	Equivalent square-formed uncollapsed height (μm)	Equivalent circle-formed uncollapsed diameter (μm)	Wall thickness(μm)
Fiber 1	24	9.64	65.87	16.8	21.4	4.8
Fiber 2	42	14.2	138.2	28.1	35.8	7.1
Fiber 3	40	9.59	53.27	24.8	31.6	4.8

were defined on the opposed surfaces of lumen to allow contact between opposing surfaces during fiber collapse. The external compressive load is modeled by prescribing downward motion of the upper compression instrument surface. The total downward displacement was 85% of uncollapsed height of the fiber,

RESULTS

Single-cycle compression tests were performed on three fibers, the results of which are summarized in Table 1. Finite element models of these three fibers were developed based on the dimensions of equivalent square-formed and circle-formed uncollapsed cross-sections, also shown in Table 1.

For fiber 1, the modeled deformed shapes with Von-Mises stress distributions for three states of collapse are shown in Fig. 5. Each of the color zones has stresses lying between the values at either end of the corresponding zone in the legend. In both the square- and circle-formed models, regions of high stress develop at each end of the lumen. In the square-formed model, these regions are in the form of columns that support a large compressive load. The curvature of the circle-formed model suppresses the development of these regions of high compressive stress as the sidewalls readily deflect in the lateral direction.

In these plots, the thickness of the fully collapsed fiber appears to be less for the circle-formed fiber than for the square-formed fiber. These thicknesses are, in fact, equivalent. The apparent differences are due to scaling of the plots.

The experimental and numerical force/displacement curves for fiber 1 are shown in Fig. 6. The curve for the square-formed model lies well above the circle-formed model. This is consistent with the development of load-bearing columns in the square-formed model versus bending and lateral deflection at the ends of the lumen in the circle-formed model. The experimental curve lies between the square- and circle-formed models.

The modeled collapse behavior of fibers 2 and 3 was similar to the behavior of fiber 1. The stress contours exhibited similar characteristics and the force versus displacement curves for the circle-formed and square-formed geometries form lower and upper bounds, respectively, on the experimental curves. The data for these fibers are not included here.

Parametric studies of the effects of fiber-wall thickness, uncollapsed fiber diameter, and elastic modulus were also performed. The study of fiber-wall thickness was based on a circle-formed fiber with an initial diameter of 30 microns and an elastic modulus of 53.27 MPa (taken from fiber no. 3). The fiber-wall thickness was varied from 3 microns to 7 microns.

The slope of the region of lumen collapse and the collapse force (F_c) both increase as wall thickness increases, as shown in Fig. 7. The increasing slope in the region of lumen collapse is due to the increasing resistance to bending of the cell wall. The increasing slopes in this region lead inevitably to higher forces at collapse.

The study of the effects of uncollapsed fiber diameter was based on a circle-formed fiber with uncollapsed diameters of 20, 30, and 40 microns, a wall thickness of 4 microns, and an elastic modulus of 65.87 MPa (taken from fiber no. 1). As shown in Fig. 8, the slope of the lumen collapse region and the collapse force both decrease as uncollapsed diameter increases.

Collapse of the fiber is controlled largely by the resistance to "hinging" at the extreme lateral

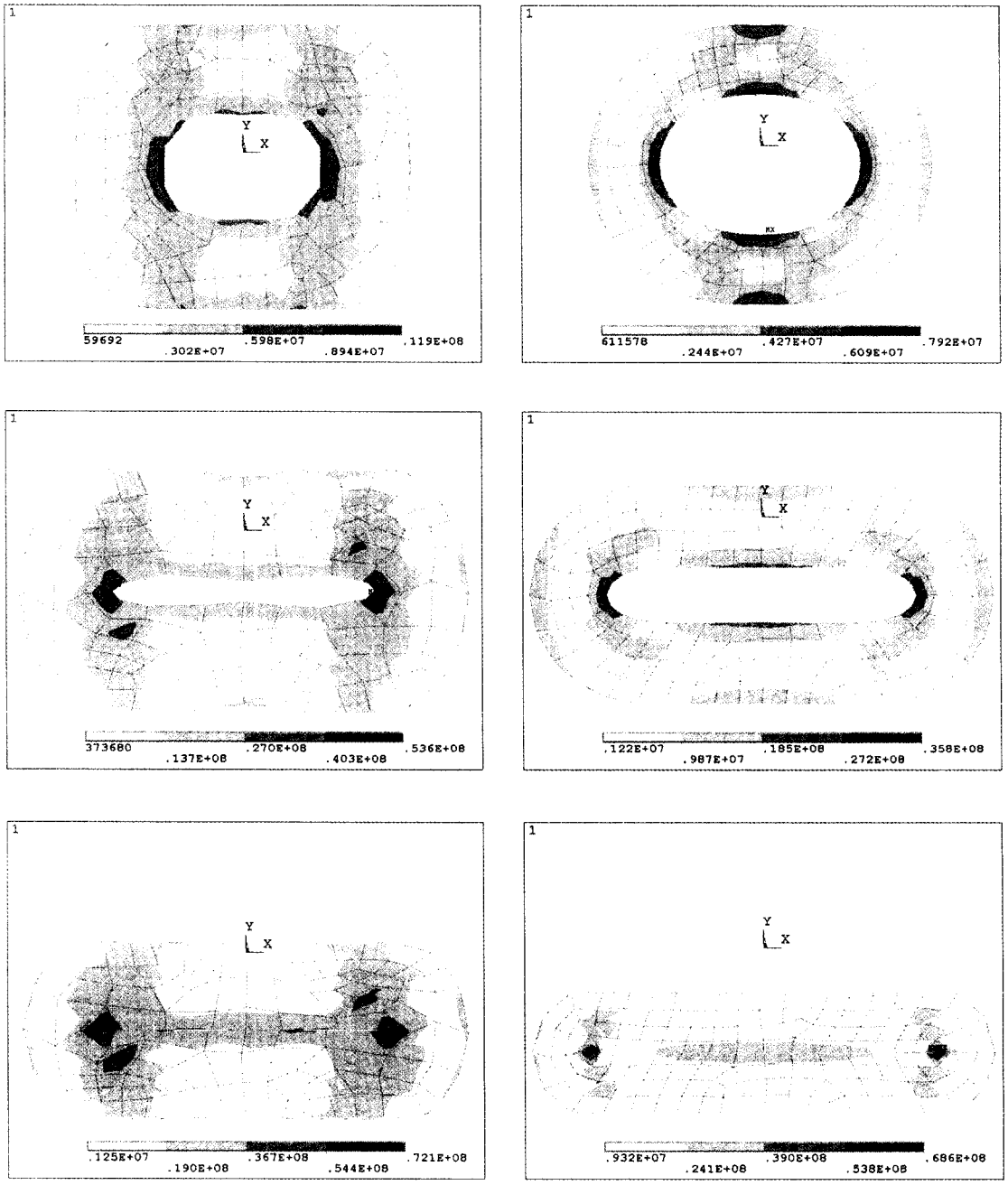

FIG. 5. For fiber 1, collapse of (a) square-formed model and (b) circle-formed model showing Von-Mises stress (Pa) distributions through the fiber wall.

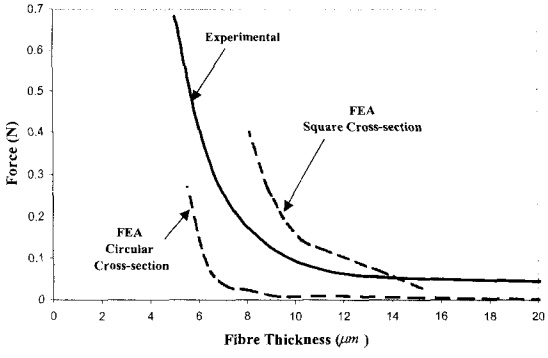

FIG. 6. Comparison of experimental FEA force/displacement curves for fiber 1.

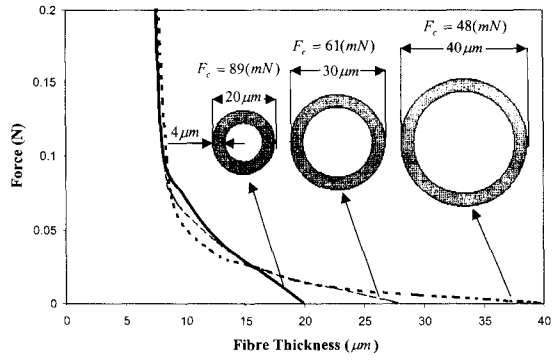

FIG. 8. Effect of initial fiber diameter of collapse behavior (E = 65/87 MP_a).

ends of the lumen, as illustrated in Fig. 5. Consider the fiber divided by a vertical axis of symmetry. For each half of the fiber, there is a resultant vertical force. The product of this force with the "moment arm" from this force to the midpoint of the fiber wall, at the extreme ends of the lumen, defines the moment that leads to hinging. As fiber diameter increases, this moment arm increases, leading to lower slopes in the lumen collapse region and lower collapse forces.

The study of the effects of elastic modulus was based on a circle-formed fiber with an uncollapsed diameter of 30 microns and a wall thickness of 4 microns. As shown in Fig. 9, the slope of the lumen collapse region, the slope in the cell-wall compressions region, and the collapse force (F_c) increase as modulus increases. This is consistent with the stiffening of the fiber structure that results from a higher modulus.

CONCLUSIONS

The collapse of behavior of individual pulp fibers has been modeled using nonlinear finite element analysis. The model geometries and material properties are based on experimental data taken from compression tests of individual fibers. The initial uncollapsed geometry of the fibers is unknown but is assumed to be either square or circular. The cell wall is assumed to be homogenous, isotropic, and linearly elastic. The results of the square-formed and circle-formed models provide upper and lower bounds on the

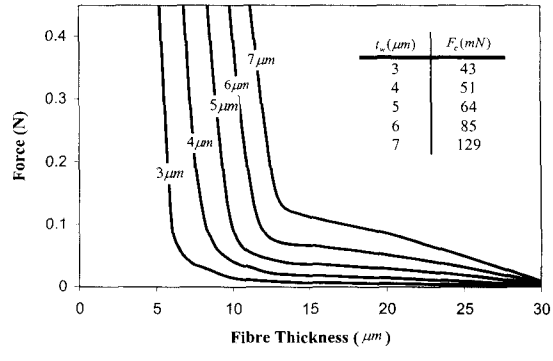

FIG. 7. Effect of fiber wall thickness on collapse behavior (E = 53.27 MPa).

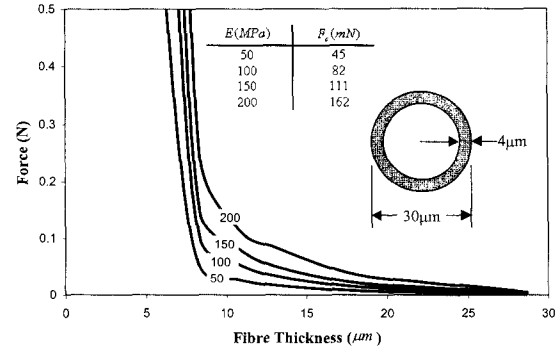

FIG. 9. Effect of equivalent elastic constant on collapse behavior.

experimental force/displacement data for all of the three fibers that were modeled. Thus, although these models are based on gross simplifications of fiber structure, material properties, and geometry, it is clear that important aspects of fiber collapse behavior have been captured. Future work will concentrate on the introduction of anisotropy, material nonlinearity, and failure criteria leading to material property degradation.

ACKNOWLEDGMENTS

The financial support of the National Centres of Excellence for Mechanical Wood-Pulps is gratefully acknowledged.

REFERENCES

AMIRI, R., AND R. HOFMANN. 2003. Dynamic compressibility of papermaking pulps. Paperi ja Puu/Paper and Timber 85(2):100–106.

DUNFORD, J. A., AND P. M. WILD. 2002. Cyclic transverse compression of single wood-pulp fibres. J. Pulp Paper Sci. 28(4):136–141.

HARTLER, N., AND J. NYRÉN. 1969. Influence of pulp type and post-treatment on the compressive force required for collapse. TAPPI Spec. Tech. Assoc. Publ. 8:265–277.

HARDACKER, K. W. 1969. Sectional area measurement of individual wood pulp fibers by lateral compaction. TAPPI J. 52(9):1742–1746.

JANG, H. F. 2001. A theory for the transverse collapse of wood pulp fibres. 12th Fundamental Research Symposium, Oxford, UK. Pp. 193–210.

———, AND R.S. SETH. 1998. Using confocal microscopy to characterize the collapse behavior of fibres. TAPPI J. 81(5):167.

LUCE, J. E. 1970. Transverse collapse of wood pulp fibers. Fiber models. TAPPI Spec. Tech. Assoc. Publ. 8:278–281.

REIZIN'SH, R. E., AND S. A. CHERNYAVSKAYA. 1975. Mechanical properties of individual fibers of wood cellulose. Pervaya Vses. Konf. Khim. Fiz. Tsellyul. (Riga) 2: 108–111.

THORPE, J., AND D. MCLEAN. 1983. Simulation of the effects of compression and shear on single fibers. TAPPI Proc. 1983 Int. Paper Phys. Conf.